J. Fluid Mech. (2003), *vol.* 497, *pp.* 381–403. © 2003 Cambridge University Press
DOI: 10.1017/S0022112003006736 Printed in the United Kingdom

Self-similar solutions for viscous capillary pinch-off

By ASIMINA SIEROU AND JOHN R. LISTER

Department of Applied Mathematics and Theoretical Physics, University of Cambridge, Centre for Mathematical Sciences, Wilberforce Road, Cambridge CB3 0WA, UK

(Received 7 May 2003 and in revised form 18 August 2003)

The axisymmetric capillary pinch-off of a viscous fluid thread of viscosity $\lambda\mu$ and surface tension γ immersed in a surrounding fluid of viscosity μ is studied. Similarity variables are introduced (with lengthscales decreasing like τ, the time to pinch-off, in a rapidly translating frame) and the self-similar shape is determined directly by a combination of modified Newton iteration and a standard boundary-integral method. A large range of viscosity ratios is studied ($0.002 \leqslant \lambda \leqslant 500$) and asymmetric profiles are observed for all λ, with conical shapes far from the pinching point, in agreement with previous time-dependent studies. The stability of the steady solutions is investigated and oscillatory instability is found for $\lambda \geqslant 32$. For $\lambda \ll 1$ an asymptotic scaling of $\lambda^{1/2}$ is suggested for the slopes of the far-field conical shapes. These compare well with the quantitative predictions of a one-dimensional theory based on Taylor's (1964) analysis of a slender bubble.

1. Introduction

The break-up of a liquid thread under the influence of capillary forces has been the subject of numerous theoretical and experimental studies over the past decade, motivated by both industrial applications (e.g. spraying, emulsification, ink-jet printing) and theoretical interest in topological transitions. In recent years theoretical studies have concentrated on a local analysis of the fluid motion near the point where the thread pinches off; such an approach is possible since close to the breaking point the relevant lengthscales and timescales are orders of magnitude smaller than those in the bulk flow. Self-similar solutions that describe the evolution towards (and after) the singularity can thus be found.

Eggers (1993), neglecting the influence of the external or ambient fluid, derived a long-wavelength approximation to the Navier–Stokes equations and found a self-similar solution that is controlled by a balance between surface tension, viscosity and inertia. Papageorgiou (1995) dropped inertia from the long-wavelength approximation and described self-similar solutions for a single fluid with a viscous–capillary balance. Brenner, Lister & Stone (1996) extended these results to an infinite family of similarity solutions in each case. Chen & Steen (1997), Day, Hinch & Lister (1998) and Leppinen & Lister (2003) investigated the limit of an inertia–capillary balance for break-up in potential flow with one or two fluids; this balance gave solutions with equal radial and axial scales which can no longer be described by a long-wavelength approximation. Lister & Stone (1998) reintroduced viscous drag in the external fluid and argued that sufficiently close to break-up the generic dominant balance is between

https://doi.org/10.1017/S0022112003006736 Published online by Cambridge University Press

capillary pressure and the internal and external viscous stresses with inertia becoming negligible. Moreover, they obtained numerical evidence of self-similar behaviour near pinching by studying the relaxation of an extended axisymmetric drop pinching in an ambient fluid of the same viscosity. Zhang & Lister (1999) confirmed the same self-similar scalings, in which all lengthscales decrease like the time to pinch-off τ, in numerical simulations for the case of two fluids of different viscosities, while experiments by Cohen *et al.* (1999) and Cohen & Nagel (2001) also demonstrated this behaviour.

Although the work of Zhang & Lister (1999) and Cohen *et al.* (1999) verified the existence of self-similar solutions over a range of viscosity ratios λ between the inner and outer fluid, a number of questions remained open. The behaviour in the limits $\lambda \ll 1$ and $\lambda \gg 1$ (corresponding to the pinching of a bubble in a viscous fluid and of a viscous fluid in air) was never fully resolved and no convincing asymptotic scaling with λ was found. The time-dependent simulations of Zhang & Lister (1999) converged to a steady self-similar shape for $\lambda = 1, 2, 4, 8, 16$ but gave oscillatory behaviour for $\lambda = 32$ onwards; the cause of the oscillations, physical or numerical, was unclear and the stability of the solutions was not investigated further. Their results did show self-similarity with all lengths scaling like τ up to viscosity ratio $\lambda = 16$, suggesting that the limit $\lambda \gg 1$ might contrast with the scalings found by Papageorgiou (1995) for a single viscous fluid pinching in vacuum ($\lambda = \infty$), for which the axial scale is $\tau^{0.175}$.

The purpose of this work is to extend the previous results to a much greater range of λ, using an alternative numerical formulation, and attempt to address some of the unresolved issues in the limits of very large and very small viscosity ratios. Most of the studies of pinching with two fluids have concentrated on calculating solutions at successive times approaching the singularity, until a self-similar regime is reached. Such an approach confirms the suggested scalings with time, but can become prohibitively expensive as the lengthscales near pinch-off become vanishingly small. Alternatively, the self-similar scalings can be used to incorporate the time-dependence into a similarity formulation and thus obtain self-similar solutions directly. This approach, also used by Cohen *et al.* (1999) for the special case of equal viscosity ($\lambda = 1$) fluids, is followed here for a large range of viscosity ratios λ, and the time-dependent results of Zhang & Lister (1999) for $1/16 \leqslant \lambda \leqslant 16$ are thus extended to $0.002 \leqslant \lambda \leqslant 500$. Access to a wider range of viscosity ratios allows us to study the asymptotic limits of very large and very small λ in more detail. In addition, the self-similar formulation provides a valuable tool to examine the stability of the similarity solutions (Witelski & Bernoff 1999; Leppinen & Lister 2003); it is thus shown that the steady similarity solutions become unstable for $\lambda > 32$.

In the next section we outline the self-similar formulation and the combination of an iterative scheme and the boundary-integral method that is used to determine the solution. The non-local component of the axial velocity, first observed by Lister & Stone (1998), is also discussed, and appropriately incorporated into the solution. In § 3 the self-similar profiles for viscosity ratios ranging from 0.01 to 500 are discussed and compared with the time-dependent and experimental results. In § 4 a simple long-wavelength model for a fluid pinching in a much more viscous ambient environment is presented ($\lambda \ll 1$) and a $\lambda^{1/2}$ scaling is proposed for the slopes of the far-field conical shapes. The stability of the steady solutions is discussed in § 5, and finally discussion and conclusions are presented in § 6.

https://doi.org/10.1017/S0022112003006736 Published online by Cambridge University Press

2. Self-similar formulation

2.1. *Equations of motion*

Consider an axisymmetric fluid thread of viscosity $\lambda\mu$ and surface tension γ surrounded by a second immiscible fluid of viscosity μ. Cylindrical polar coordinates r and z are introduced and the corresponding radial and axial velocities are denoted by u_r and u_z. Assuming that Stokes flow holds in both the pinching and the surrounding fluid, the flow is described by

$$\nabla \cdot \boldsymbol{u} = 0, \tag{2.1a}$$

$$\mu_{1,2}\nabla^2 \boldsymbol{u} - \nabla p = \boldsymbol{0}, \tag{2.1b}$$

where $\mu_{1,2}(= \lambda\mu$ and $\mu)$ is the viscosity of the inner or outer fluid, as appropriate. On the two-fluid interface the velocity is continuous and the stress jumps by the capillary pressure so that

$$[\boldsymbol{u}]_S = 0 \qquad \text{and} \qquad [\boldsymbol{\sigma} \cdot \boldsymbol{n}]_S = \gamma \boldsymbol{n} \nabla \cdot \boldsymbol{n}, \tag{2.2a, b}$$

where $[\,]_S$ denotes the jump across the surface of the thread S, γ is the coefficient of surface tension, $\boldsymbol{n}$ is the outward normal and $\nabla \cdot \boldsymbol{n}$ is the surface curvature. The evolution of the interfacial position is determined from the kinematic boundary condition

$$\frac{\partial F}{\partial t} + \boldsymbol{u} \cdot \nabla F = 0, \tag{2.3}$$

where $F(r, z, t) = 0$ describes the free surface. In addition, a boundary condition for the flow far away from the pinching thread is required; e.g. no flow in the external fluid. The formulation of the appropriate far-field boundary condition will be discussed in more detail in § 2.4 in the context of the self-similar solution.

2.2. *Self-similar variables*

When only free boundaries are present there is no preferred direction in the Stokes equations; as a result, the axial and radial lengths should have the same scaling, $r \sim z$, as the time to pinch-off is approached. The balance between capillary pressure and the internal and external viscous stresses proposed by Lister & Stone (1998) further suggests that the velocity is constant as a function of time, while both r and z scale linearly with time to pinch-off. Time-dependent simulations by Lister & Stone (1998) for $\lambda = 1$ revealed that, although the shape of the pinching region followed the proposed scaling, the axial velocity increased logarithmically. This logarithmic divergence was shown to be the result of non-local contributions and, as will be discussed in detail in § 2.4, can be readily subtracted. Similarity variables can then be introduced by

$$\bar{z} = \frac{\mu}{\gamma}\frac{z}{\tau}, \qquad \bar{r} = \frac{\mu}{\gamma}\frac{r}{\tau}, \qquad \bar{\boldsymbol{u}} = \frac{\mu}{\gamma}\boldsymbol{u}, \tag{2.4a, b, c}$$

where $\tau = t_p - t$ is the time to pinch-off and it is assumed that all non-local contributions have been subtracted from the velocity $\boldsymbol{u}$. (Note that the non-dimensionalization is also included in the similarity formulation.)

For Stokes flow, the equations governing the motion of the fluid have no time dependence and therefore the functional form of (2.1)–(2.2) is still valid for the self-similar variables (but now with non-dimensional coefficients for the viscosities and the surface tension). The kinematic boundary condition is now rewritten as

$$-\bar{F} + \nabla \bar{F} \cdot \bar{\boldsymbol{r}} + \bar{\boldsymbol{u}} \cdot \boldsymbol{n} = 0 \tag{2.5}$$

https://doi.org/10.1017/S0022112003006736 Published online by Cambridge University Press

or, in a cylindrical polar coordinate frame, simply as

$$n_r(u_r + \bar{r}) + n_z(u_z + \bar{z}) = 0, \tag{2.6}$$

where $\boldsymbol{n} = (n_r, n_z) = \nabla F$ is the normal to the interface, and the overbars have been dropped from the velocities.

Note that any constant axial velocity $\gamma V/\mu$ in real space can be removed by a Galilean transformation. This invariance still holds in similarity space and simply corresponds to a displacement V along the $\bar{z}$-axis, as is apparent from (2.4*a*). In addition, a change of timescale $\tau \to \tau/C$ in real space corresponds to a scaling of the similarity variables $\bar{r}$ and $\bar{z}$ by an arbitrary constant C. Hence the minimum radius of the pinching neck can be defined to have any given value in the self-similar frame by a suitable choice of C. For any given self-similar shape defined by $(\bar{r}, \bar{z})$, one can define any number of equivalent self-similar shapes, according to $\bar{r} = C\bar{r}^\star$ and $\bar{z} = C\bar{z}^\star + V$, where C and V are arbitrary constants, corresponding to a choice of timescale and moving frame of reference in the real space. Equations (2.1)–(2.2) would still be valid for $(\bar{r}^\star, \bar{z}^\star)$, while the kinematic boundary condition would take the more general form

$$n_r u_r + n_z(u_z - V) + C(n_r\bar{r}^\star + n_z\bar{z}^\star) = 0, \tag{2.7}$$

where the normal to the interface and the velocities are not affected by the new choice of similarity transformation. Note that the choice of C and V has no physical significance for the self-similar shape and it simply defines a reference frame and timescale. If C is set equal to the radial velocity of the minimum of the pinching neck then the radial position of the minimum always stays at $\bar{r} = 1$; such a frame is used for convenience in the following calculations, and all results are presented with a pinching neck of radius 1. (No attempt is made *a priori* to fix the axial position of the minimum; for clarity, when shapes are compared, the minimum is moved to $z = 0$.)

Finally, we note here that the general time-dependent evolution of the interface can also be written in the similarity variables as

$$-\frac{\partial \bar{F}}{\partial q} = \nabla \bar{F} \cdot (\bar{\boldsymbol{r}} + \boldsymbol{u}) \equiv K, \tag{2.8}$$

where $q = -\ln\tau$ is a new temporal variable and $\bar{F} = \bar{F}(\bar{r}, \bar{z}, q)$. In this notation, self-similar solutions $\bar{F}(\bar{r}, \bar{z})$ are steady q-independent solutions of $K = 0$; the introduction of q is essential for the linear-stability analysis of § 5.

2.3. *Solution in the self-similar frame*

A standard boundary-integral formulation can be used for the solution of the Stokes equations in similarity variables. The velocity of any point $\boldsymbol{x}_s$ on the two-fluid interface can be written as (Rallison & Acrivos 1978; Stone & Leal 1990)

$$\frac{1}{2}(1+\lambda)\boldsymbol{u}(\boldsymbol{x}_s) + (1-\lambda)\int_{\boldsymbol{y}\in S} \boldsymbol{n}\cdot\boldsymbol{K}\cdot\boldsymbol{u}\,\mathrm{d}S_y = -\int_{\boldsymbol{y}\in S} (\nabla\cdot\boldsymbol{n})\boldsymbol{n}\cdot\boldsymbol{J}\,\mathrm{d}S_y, \tag{2.9}$$

where

$$\boldsymbol{J}(\boldsymbol{r}) = \frac{1}{8\pi}\left(\frac{\boldsymbol{I}}{R} + \frac{\boldsymbol{RR}}{R^3}\right), \quad \boldsymbol{K}(\boldsymbol{r}) = -\frac{3}{4\pi}\frac{\boldsymbol{RRR}}{R^5} \quad \text{and} \quad \boldsymbol{R} = \boldsymbol{x} - \boldsymbol{y}.$$

For $\lambda \neq 1$ equation (2.9) results in an algebraic system of equations (See Stone & Leal 1990 for details on the discretization of the interface and the numerical

https://doi.org/10.1017/S0022112003006736 Published online by Cambridge University Press

implementation) that can be solved for the interfacial velocities once the interfacial positions are known. The integral formulation in (2.9) assumes an integral over a closed interface, such as a finite drop, and its application in the present context, including points that are very far from the pinching region, requires some care; more details are given in § 2.4.

In the self-similar frame of reference, where the time-dependence has been eliminated, the kinematic boundary condition (2.5) can be used as a constraint to determine the asymptotically self-similar shape. An initial guess for the interfacial shape is assumed and a modified Newton scheme (see Leppinen & Lister 2003) is used for the calculation of successive shapes. The Jacobian for the Newton scheme is obtained numerically by perturbing the interface in the direction of the normal at each grid point and calculating the changes to (2.5) due to these small displacements. The interfacial velocities required to evaluate (2.5) are calculated directly from the boundary-integral formulation so that, unlike the case for potential flow, the velocities are not part of the iterative procedure. The iterative scheme is used on a discretized area surrounding the pinching neck (typically extending to a distance of about 1000 times the minimum radius on either side of the neck) and the discretized area is extrapolated smoothly to infinity using the assumption of an asymptotically conical shape. About 200 points with spacing varying smoothly from about 0.05 in the neck to about 50 at $R = 1000$ were used for the discretization.

2.4. *The far-field and axial velocity*

Lister & Stone (1998) first showed that, although the shape of the pinching region becomes self-similar as the time to singularity is approached, the axial velocity increases logarithmically. A simple surface-integral calculation confirmed that, for the case of fluids with equal viscosity, the axial velocity near the pinching region is dominated by a term proportional to $\ln(r_{min}(t)/r_{max})$, where $r_{min}(t)$ is the minimum radius of the thread and r_{max} is the size of the drop. This logarithmic term arises from contributions driven by the curvature of the region that is asymptotically intermediate between the scales of the pinching neck and the macroscopic drop. The term corresponds to a large and increasing uniform velocity, which results in pure advection but no deformation of the pinching region. (Though the velocity is unsteady and increasing, inertia remains negligible due to the decreasing lengthscales, and the uniform advection can be removed by change of reference frame without affecting the governing Stokes equations.)

Similar conclusions can be derived for the case of two fluids of different viscosities. Separable solutions for the Stokes flow driven by surface tension on two perfect infinite cones can be obtained analytically and a logarithmic term in the axial velocity is found for arbitrary values of λ. (The details of the calculation are in the Appendix.) Note that for the case of infinite cones the axial velocity includes a term logarithmic in the distance, $R = (r^2 + z^2)^{1/2}$, from the cone tip that diverges as $R \to 0$ or $R \to \infty$. For the time-dependent problem studied by Lister & Stone (1998), a macroscopic lengthscale r_{max} exists and the shape is only conical for $r_{min}(t) \ll R \ll r_{max}$. The logarithmic contribution to the axial velocity, driven by the conical region, then scales as $\ln(r_{min}(t)/r_{max})$.

Zhang & Lister (1999) dealt with the logarithmic divergence of the axial velocity by truncating the conical regions at an arbitrary distance, attaching caps at the end of the cones and subtracting the resulting axial velocity of the pinching region. This approach could also be used for the case of self-similar variables; the axial velocities,

https://doi.org/10.1017/S0022112003006736 Published online by Cambridge University Press

however, would depend on the truncated distance, and the whole conical region (and the cap) would need to be discretized for the calculation of the surface integrals.

An alternative approach, followed here, is to attach open cones to the truncated domain. These cones, that now extend to an arbitrarily large distance R_∞, need not be discretized; their velocity can be calculated from the velocities within the discretized region, combined with the analytical solution for perfect cones (Appendix). The radial velocity far from the tip/pinching region is constant (and independent of the distance from the tip/pinching region), while the axial velocity has a constant contribution, plus a known logarithmic dependence given in (A 7). The velocities on the conical extension will thus be

$$u_r(R > R_{ext}) = u_r(R = R_{ext}), \qquad R_{ext} \leqslant R \leqslant R_\infty, \tag{2.10a}$$

$$u_z(R > R_{ext}) = u_z(R = R_{ext}) + A_1 \ln(R/R_{ext}), \qquad R_{ext} \leqslant R \leqslant R_\infty, \tag{2.10b}$$

where R_{ext} is the last discretized point (typically at $R \approx 1000$) and A_1 is given by (A 5). Equation (2.10) can be included in the boundary-integral formulation in a straightforward manner, by evaluating the corresponding integrals (on the extended cone) analytically and appropriately adjusting the coefficients of the discretized points. The resulting solutions still depend on R_∞, the truncation distance of the added conical region, and in order to remove this dependence $A_1 \ln(R_\infty)$ is subtracted from the axial velocity everywhere on the interface. This approach allows the calculation of velocities that are independent of truncation distance and consistent with the analytical results for perfect cones. Note, however, that the axial velocity is only determined to within an arbitrary constant, since an axial translation can always be added to the Stokes solution.

3. Results

Self-similar solutions were calculated for a wide range of λ ($0.002 \leqslant \lambda \leqslant 500$). An initial guess for $\lambda = 1$ was obtained from the time-dependent solution of Zhang & Lister (1999) and a continuation procedure was used to calculate solutions for all other values of λ.

3.1. *Velocity profiles*

The asymptotic far-field velocity profiles, calculated in the Appendix as a function of the viscosity ratio λ and the far-field cone angles, can be compared with the numerical results. A typical interfacial velocity profile, showing both the radial u_r and axial u_z components, is presented in figure 1 for $\lambda = 2$. The radial velocity far from the pinching region tends to a constant (figure 1*a*), in accordance with the asymptotic result for two perfect cones, since the surface of each cone corresponds to a fixed angle and value of $\xi = \cos\theta$ in (A 7*b*). In addition, the calculated values of u_r in the far field ($u_r = -0.0011$ for the shallow cone and $u_r = -0.0065$ for the steep one) are in excellent agreement with the values calculated from (A 7*b*) ($u_r = -0.00113$, and -0.00651 respectively, for $\theta_1 = 4.966^\circ$ and $\theta_2 = 79.5^\circ$).

As discussed in § 2.4, the dominant term in the axial velocity profile is logarithmic in R and is a result of a 'tug-of-war' between the two conical far-field regions. A logarithmic best-fit to the numerical profile is presented in figure 1(*b*) and it is apparent that it accurately describes the interfacial velocities in the far field. The fitted coefficient of the logarithmic term (0.0153) is in very good agreement with the value predicted by (A 5) (0.0154) and, as predicted, has the same value for both cones. According to (A 7*a*) the next term in the axial velocities is a constant; although the

https://doi.org/10.1017/S0022112003006736 Published online by Cambridge University Press

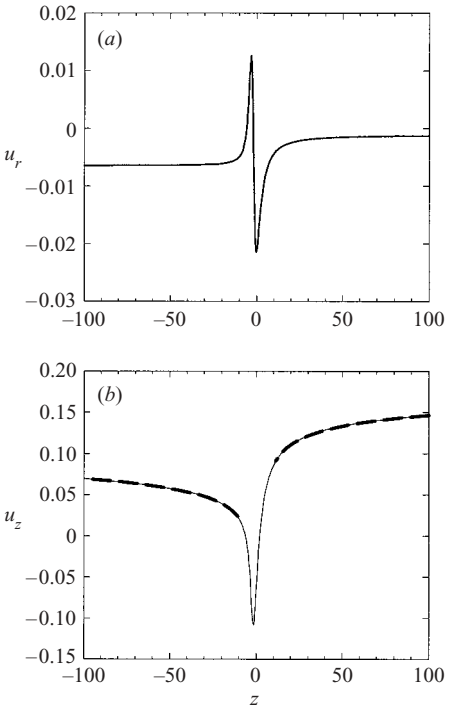


FIGURE 1. The radial (a) and axial (b) velocities on the interface for $\lambda = 2$, plotted as a function of axial distance z from the minimum radius. The dashed lines in (b) are best-fits of the form $A + B\ln(R)$. The value of B and the difference in values of A agree with (A 7).

absolute value on each cone cannot be calculated since a constant axial velocity can always be added to the problem, the difference between the constants on the two cones is again in excellent agreement between the fit to the boundary-integral calculation and the analytical approach (0.1044 and 0.1041 respectively). The excellent agreement between the far field of the numerical calculations and the asymptotic results for the perfect cones justifies the procedure described in § 2.4 for obtaining solutions on a truncated domain that are independent of the truncation distance.

The radial velocity at the minimum of the pinching neck is shown as a function of λ in figure 2; this velocity defines the timescale C in the calculations and can be compared with experimental measurements of pinching rates (see also Zhang & Lister 1999).

3.2. *Shapes*

The converged shapes of some self-similar profiles are presented in figure 3. Since the axial position of the pinching neck is arbitrary, all shapes are presented in a frame of reference with $r_{min} = 1$ and $z(r_{min}) = 0$. As has been observed in previous studies, pinching always occurs asymmetrically, while the shape on either side of the pinching region is indeed conical. The agreement between the time-dependent shapes of Zhang & Lister (1999) and the self-similar shapes calculated here is excellent and a sample comparison for $\lambda = 2$ is presented in figure 4.

The calculated slopes for the cones far from the pinching point are presented in figure 5 and compared with the time-dependent results of Zhang & Lister (1999) and the experimental results of Cohen *et al.* (1999) and Cohen & Nagel (2001). The slope

https://doi.org/10.1017/S0022112003006736 Published online by Cambridge University Press

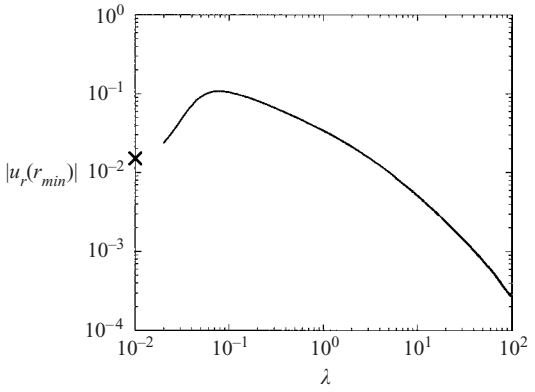


FIGURE 2. The radial velocity at the minimum of the pinching neck (i.e. the self-similar pinching rate $\mathrm{d}h_{min}/\mathrm{d}t$) as a function of the viscosity ratio λ. This defines the timescale C in (2.7) such that the self-similar minimum radius is 1. The cross denotes the limit value of $\mathrm{d}h_{min}/\mathrm{d}t$ as $\lambda \to 0$, calculated from the long-wavelength approximation of §4, and is given by $\mathrm{d}h_{min}/\mathrm{d}t = (\tilde{C}/2)H_{min}$.

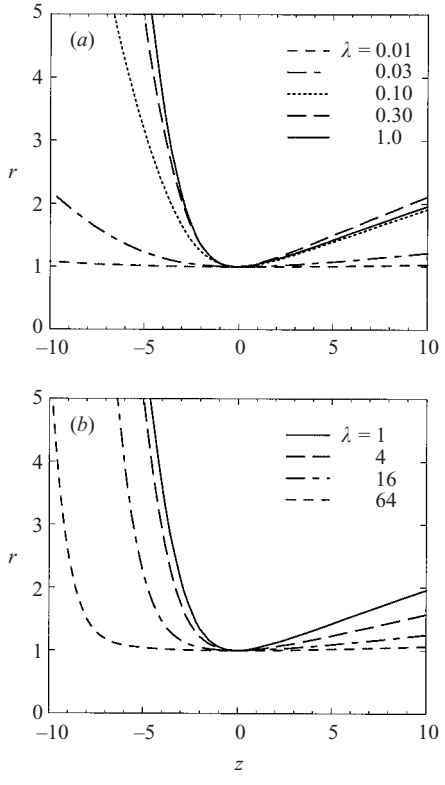


FIGURE 3. The shape of the pinching region as a function of the viscosity ratio λ (*a*) for $\lambda \leqslant 1$ and (*b*) for $\lambda \geqslant 1$.

S_+ of the steep cone increases monotonically with λ, while the slope S_- of the shallow cone peaks near $\lambda = 0.5$ and decreases as $\lambda \to 0$ or ∞. Unresolved discrepancies between the earlier experimental and numerical results for $\lambda \ll 1$ were discussed in both Zhang & Lister (1999) and Cohen & Nagel (2001). The self-similar solutions

https://doi.org/10.1017/S0022112003006736 Published online by Cambridge University Press

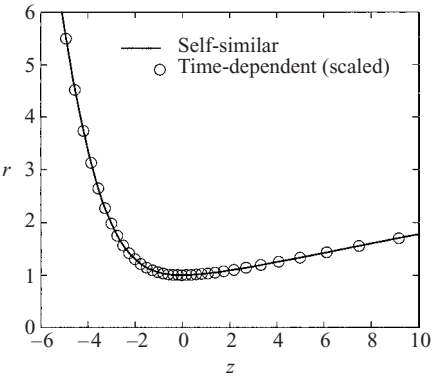


FIGURE 4. The shape of the pinching region for $\lambda = 2$ compared with the converged scaled shape from the time-dependent calculations of Zhang & Lister (1999). Similar excellent agreement is found for other values of λ.

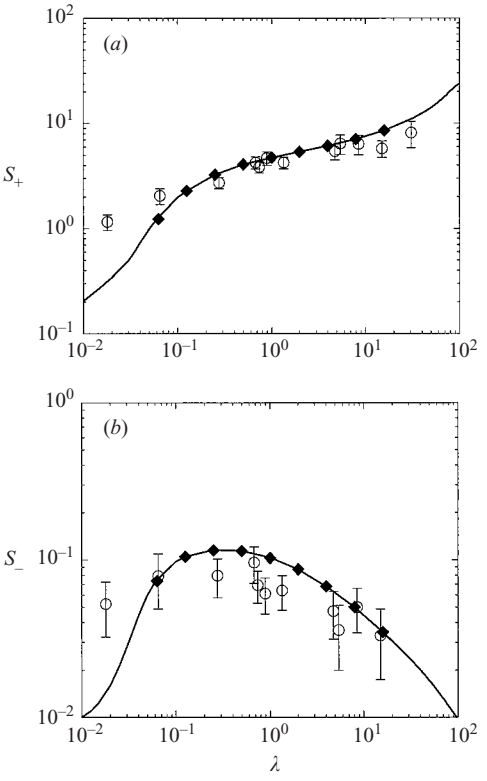


FIGURE 5. The slopes of the far-field cones as a function of λ (solid line), compared with the experimental measurements of Cohen *et al.* (1999) (open circles and error bars) and the time-dependent results of Zhang & Lister (1999) (filled diamonds): (*a*) steep cone slope S_+ and (*b*) shallow cone slope S_-. Only the range of λ where experimental results are available is shown.

calculated directly here give excellent agreement with the time-dependent results of Zhang & Lister (1999) in the region of overlap, and they confirm and extend the trend for $\lambda \ll 1$.

https://doi.org/10.1017/S0022112003006736 Published online by Cambridge University Press

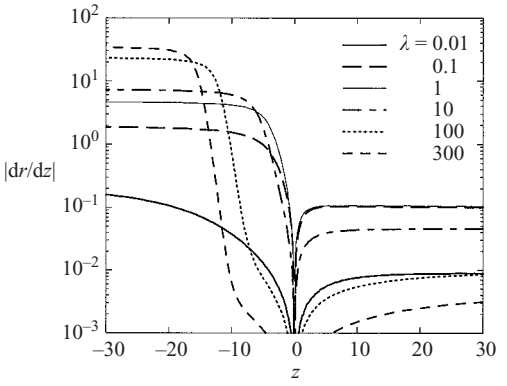


FIGURE 6. The slopes of the self-similar shapes as a function of axial distance z from the minimum radius. Convergence to the constant slopes of the far-field cones is slower for $\lambda \ll 1$ and $\lambda \gg 1$.

The discrepancies between the results of Zhang & Lister (1999) and Cohen *et al.* (1999) for small values of λ, along with experimental and computational difficulties encountered for both $\lambda \ll 1$ and $\lambda \gg 1$, did not allow the previous work to determine accurately any asymptotic trends for either large or small values of the viscosity ratio. As can be seen in figure 5, for $\lambda \ll 1$ both cone angles approach zero, subjecting their experimental evaluation to potentially large errors. The same is true for $\lambda \gg 1$ where now one angle approaches zero, while the other one approaches 90°.

In figure 6 we show the slopes of the interface as a function of axial position for different values of λ. It is apparent that the rate of convergence to the asymptotic slopes is slower for both large and small λ, which may be an important constraint on experimental measurements.

Zhang & Lister (1999) observed oscillations in the time-dependent behaviour and were unable to find self-similar solutions for $\lambda > 16$. The direct calculation in similarity variables used here, together with the improved treatment of the far field, is subject to fewer limitations and our calculations can thus be continued for much smaller and larger values of the viscosity ratio. A detailed analysis of the case $\lambda \ll 1$ is presented in § 4, while a stability analysis that explains the limitation of experiments for large λ is presented in § 5. Leaving questions of stability aside for the moment, we discuss the self-similar solution for $\lambda \gg 1$ (e.g. a very viscous fluid pinching in air) in the following section.

3.3. *The case* $\lambda \gg 1$

The converged self-similar shapes for $100 \leqslant \lambda \leqslant 400$ are presented in figure 7, and the corresponding far-field cone slopes are presented in figure 8 as a function of λ. As λ is increased the slope of the steep cone increases monotonically, while the slope of the shallow cone decreases monotonically; the overall shape of the pinching region resembles a cylindrical thread attached to a bulb as the steep cone angle approaches 90° and the shallow cone angle approaches zero. Moreover, as λ increases the axial distance between the point of minimum radius and the start of the steep cone also increases (figure 7). In order to quantify this change, we define a characteristic axial lengthscale Z_d equal to the axial distance between the position of the minimum radius ($z = 0$ in our frame) and the position of the maximum axial curvature. The axial curvature, $\kappa_2(z) = \mathrm{d}^2r/\mathrm{d}z^2[1 + (\mathrm{d}r/\mathrm{d}z)^2]^{-3/2}$, is shown in figure 9 for different λ. The dependence of Z_d on λ is plotted in figure 10(*a*) and compared with the corresponding

https://doi.org/10.1017/S0022112003006736 Published online by Cambridge University Press

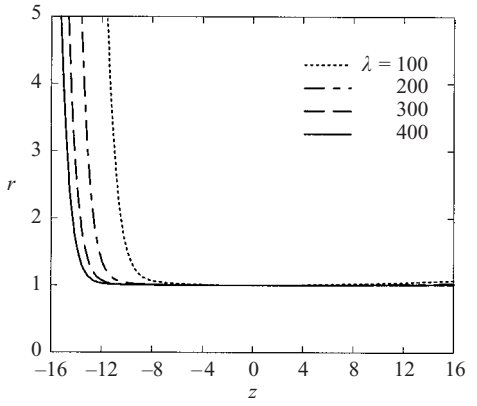


FIGURE 7. The shape of the pinching region as a function of the viscosity ratio λ for large λ. The minimum radius is at $z = 0$ and the start of the steep cone shifts to positions further away from the minimum radius as λ increases.

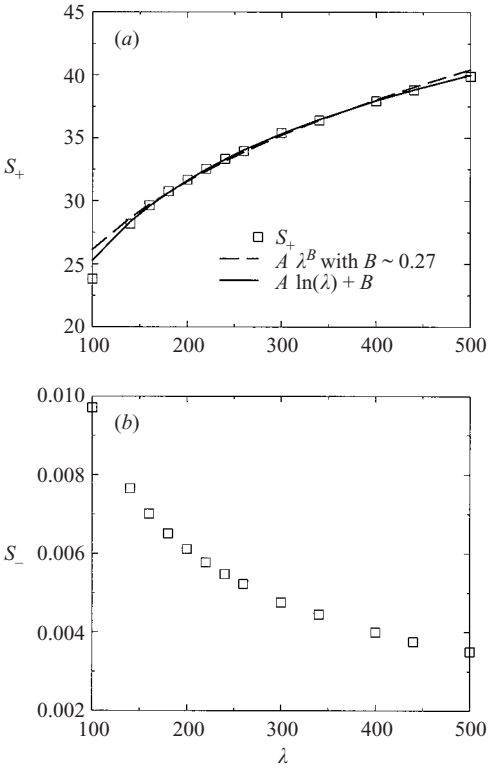


FIGURE 8. The steep and shallow cone slopes plotted as functions of λ, for $\lambda \geqslant 100$. Empirical fits of the form $A\lambda^B$ with $B \approx 0.27$ and $A\ln(\lambda) + B$ are shown for the steep slope S_+.

steep cone slope S_+; both appear to be similarly slowly increasing functions of λ. In figure 10(*b*), the steep cone slope is plotted as a function of Z_d; all points for $\lambda > 100$ lie on a straight line, suggesting that the steepening of the slope and the increase of the lengthscale of the thread might be related.

https://doi.org/10.1017/S0022112003006736 Published online by Cambridge University Press

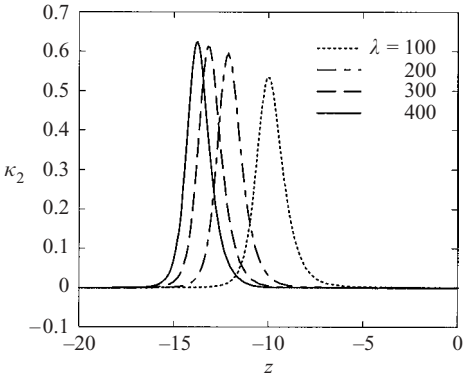


FIGURE 9. The axial curvature κ_2 as a function of axial distance z, for different values of λ.

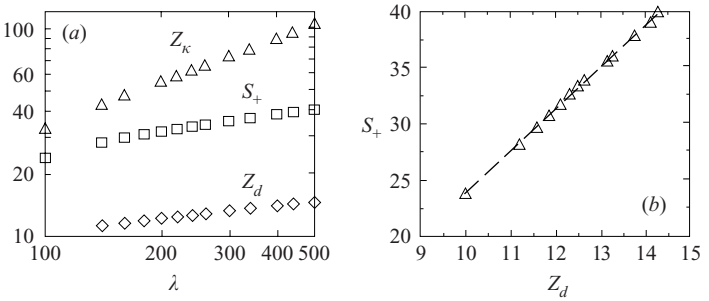


FIGURE 10. The variation of the steep cone slope S_+ with characteristic lengthscales associated with the axial curvature: (*a*) Z_d, the axial distance of the maximum axial curvature from the minimum radius, and $Z_\kappa = [r(0)/\kappa_2(0)]^{1/2}$, the lengthscale defined by the axial curvature at the minimum radius. Z_d and Z_κ appear to define two distinct and independent lengthscales which approximately scale as $\lambda^{0.24}$ and $\lambda^{0.67}$ for the range $200 \leqslant \lambda \leqslant 500$. The steep cone slope S_+ is also shown for comparison. (*b*) S_+ plotted as a function of Z_d (open triangles); a best linear fit is also shown (dashed line).

The axial length Z_d, however, is not the only axial lengthscale in the problem. The axial curvature at the minimum radius also defines a characteristic lengthscale $Z_\kappa = [r(0)/\kappa_2(0)]^{1/2}$ (also shown in figure 10*a*) which scales differently from Z_d. The existence of at least two axial lengthscales further complicates any understanding of the steepening of the steep cone for large λ.

Theoretical prediction of the functional dependence of either slope on λ is unfortunately not straightforward. A simplified asymptotic model successfully describing pinching of a very viscous thread surrounded by a much less viscous fluid has yet to be developed. As shown above, attempts to develop such a model are complicated by the increase of the steep cone slope as a function of λ, so that a simple long-wavelength approach is inappropriate, and by the presence of at least two lengthscales. Prior to these results, Lister & Stone (1998) suggested a simple slender-body analysis for $\lambda \gg 1$ which balanced external shear stress and internal extensional stress to predict that the slenderness ratio ϵ of the radial to axial scales should scale as $\epsilon|\ln\epsilon| \sim \lambda^{-1/2}$ as $\lambda \to \infty$. Although this scaling obviously fails to describe the behaviour of the steep cone, it does seem to predict the flattening of the shallow cone. In figure 11 we plot $S_-|\ln S_-|$ against λ; the data are described satisfactorily by a fit of the form $A/\lambda^{1/2}$. No theoretical predictions are available for

https://doi.org/10.1017/S0022112003006736 Published online by Cambridge University Press

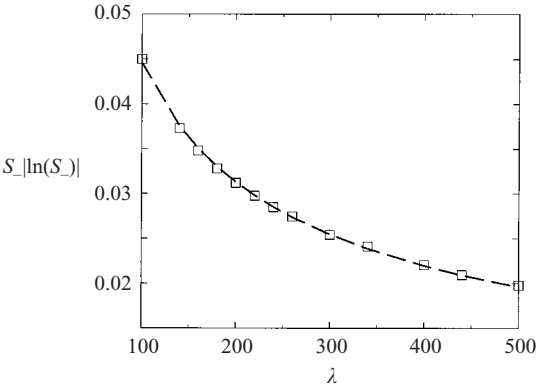


FIGURE 11. $S_-|\ln S_-|$ as a function of λ (open squares); a fit of the form $A\lambda^{-1/2}$ is also shown (dashed line).

the behaviour of the steep cone slope, which could be described reasonably well by either a power-law fit $A\lambda^B$ or the form $A\ln\lambda + B$ (figure 8*a*). In the absence of a theoretical justification, these are, however, only empirical fits.

Finally, it is worth mentioning that previous solutions by Papageorgiou (1995) for the pinching of a viscous thread in the absence of an external fluid ($\lambda = \infty$) showed that the local profiles near pinch-off are symmetric about the pinch point. This seems surprising in the light of our present results (and previous results by Zhang & Lister 1999; Cohen *et al.* 1999 and Pozrikidis 1999), where the degree of asymmetry increases markedly with λ, for values of λ up to at least 500. In addition, Papageorgiou (1995) shows that the axial lengthscale for $\lambda = \infty$ varies as $z \sim \tau^{0.175}$ rather than $z \sim \tau$ as found here for all finite λ. The observed behaviour for large λ suggests that the limits $\lambda \to \infty$ and $\tau \to 0$ do not commute so that the symmetric self-similar solution for a single fluid does not describe the proper asymptotic solution as $\tau \to 0$ for finite λ, however large. Time-dependent simulations for relatively large λ by Pozrikidis (1999) ($\lambda = 20$), and by ourselves, show that an initially symmetric pinching neck quickly develops a central bulge and two highly asymmetric pinching necks on either side, each of which is described by the similarity solutions derived here.

4. The limit $\lambda \ll 1$

The results presented in § 3.2 suggest that as $\lambda \to 0$ the cone angles both tend to zero so that the shape of the pinching drop resembles a long thread and the axial lengthscale becomes much greater than the radial. This observation suggests that it should be possible to develop a simple one-dimensional asymptotic model to describe the pinch-off region as $\lambda \to 0$. Such an analysis would complement the numerical solutions and provide the appropriate scaling for the cone slopes as $\lambda \to 0$. The analysis below follows the insight of Taylor (1964), who realized that a large extension of a low-viscosity bubble by strain in a very viscous fluid can be described by lubrication theory for the internal flow and a line distribution of sinks for the external flow.

Consider a long thread of slowly varying radius $h(z, t)$, viscosity $\lambda\mu$ and surface tension γ immersed in an ambient fluid of viscosity μ, where now $\lambda \ll 1$. Since the radial lengthscale is significantly smaller than the axial, a simple lubrication type approach can be used to describe the flow inside the thread. Let the typical

https://doi.org/10.1017/S0022112003006736 Published online by Cambridge University Press

scale of $\partial h/\partial z$ be $\epsilon \ll 1$, so that the radial and axial scales satisfy $r \sim \epsilon z$. Mass conservation within the thread then requires that the internal velocities scale as $u_r \sim \epsilon u_z$, while the z-component of the momentum equation gives a pressure that scales as $p \sim \lambda\mu u_z/(\epsilon^2 z)$. Since the shear stress in lubrication flow scales as $\sigma_{rz} \sim \epsilon p$, the stress exerted by the inner fluid on the outer is largely radial. Hence the velocities in the outer fluid follow the scaling $u_z \sim \epsilon u_r$.

In order to specify the dependence of ϵ on λ, the normal-stress balance is used. The internal pressure in the thin thread is balanced by the sum of the capillary stress on the interface and the external viscous normal stress. If both these stresses are important then

$$p \sim \frac{\gamma}{h} \sim \mu \left(\frac{\partial u_r}{\partial r} \right)_{h_+},$$

where $(\,)_{h_+}$ denotes values just in the surrounding fluid. Thus, using the previous scalings,

$$\lambda\mu \frac{u_z}{\epsilon^2 z} \sim \frac{\gamma}{\epsilon z} \sim \mu \frac{u_z}{z}$$

which results in $\epsilon \sim \lambda^{1/2}$ and scalings

$$r/z \sim \lambda^{1/2}, \tag{4.1a}$$

$$u_r \sim \gamma/\mu \sim O(1), \tag{4.1b}$$

$$u_z \sim (\gamma/\mu)\lambda^{-1/2} \qquad (r < h) \tag{4.1c}$$

$$u_z \sim (\gamma/\mu)\lambda^{1/2} \qquad (r > h). \tag{4.1d}$$

Since $r/z \sim \lambda^{1/2}$, the slopes of the resulting cones on either side of the pinching neck will also scale as $\lambda^{1/2}$.

In addition to the simple scaling, one can also use lubrication analysis in more detail to calculate the shape of the interface exactly and obtain the values of the asymptotic slopes of the two cones. Returning to dimensional variables and using lubrication theory inside the thin thread gives

$$u_z = \frac{1}{4\lambda\mu} \left(\frac{\partial p}{\partial z} \right) (r^2 - h^2) + u_z(r = h). \tag{4.2}$$

Now $u_z(r = h)$ can be neglected by (4.1d) and continuity with the external flow. Thus the internal flux is $-(\pi h^4/8\lambda\mu)(\partial p/\partial z)$ and conservation of mass results in

$$h \frac{\partial h}{\partial t} = \frac{1}{16\lambda\mu} \left[\frac{\partial}{\partial z} \left(h^4 \frac{\partial p}{\partial z} \right) \right]. \tag{4.3}$$

In order to use (4.3) to calculate the interfacial shape, an approximation for the pressure is needed. From the normal-stress balance with $|\partial h/\partial z| \ll 1$ the pressure in the thread is

$$p = \frac{\gamma}{h} - 2\mu \left(\frac{\partial u_r}{\partial r} \right)_{h_+}. \tag{4.4}$$

Approximating the external flow as a line sink flow generated by the collapse of the pinching thread gives an external radial velocity

$$u_r = \frac{\partial h}{\partial t} \frac{h}{r},$$

https://doi.org/10.1017/S0022112003006736 Published online by Cambridge University Press

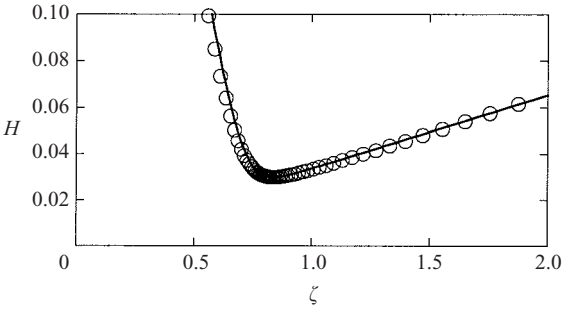


FIGURE 12. The solution of the asymptotic equation (4.8) for $\tilde{C} = 1$ (solid line) compared with the rescaled solution of the full problem for $\lambda = 0.015$ (open circles).

which, combined with (4.4), results in

$$p = \frac{\gamma}{h} + \frac{2\mu}{h}\frac{\partial h}{\partial t}. \tag{4.5}$$

Then (4.3) can be written as a partial differential equation for h,

$$h\dot{h} = \frac{1}{16\lambda}\frac{\partial}{\partial z}\left[h^4\frac{\partial}{\partial z}\left(\frac{\gamma/\mu + 2\dot{h}}{h}\right)\right], \tag{4.6}$$

where all quantities are still dimensional and $\dot{h}$ denotes $\partial h/\partial t$.

As was the case for arbitrary λ, self-similar variables can be defined, but now the partial differential equation for $h(z, t)$ can be rewritten as an ordinary differential equation for the self-similar shape. Combining the non-dimensionalization, self-similar and lubrication scalings, we define new variables H and ζ, by

$$h(z, t) = \frac{\gamma\tau\tilde{C}}{2\mu}H(\zeta), \tag{4.7a}$$

$$z = \frac{1}{(8\lambda)^{1/2}}\frac{\gamma\tau\tilde{C}}{2\mu}\zeta, \tag{4.7b}$$

where $\tilde{C}$ is an arbitrary constant that, as in § 2.2, corresponds to a choice of timescale. Then (4.6) leads to the ordinary differential equation

$$\tilde{C}H(H - H'\zeta) = \left(H^4\left(\frac{1 + \tilde{C}(H - H'\zeta)}{H}\right)'\right)'. \tag{4.8}$$

Although the equation is simplified when $\tilde{C} = 1$, it is easier to find solutions for other values of $\tilde{C}$ by using the solutions of the full problem as initial guesses; solutions for all values of $\tilde{C}$ can then be obtained by rescaling. Equation (4.8) is solved using a Newton iteration scheme; the computational cost for solution of this asymptotic small-λ problem is, however, significantly smaller than the cost for solving the full problem of § 2.3, since it is no longer necessary to calculate the velocities from the boundary-integral equation. As in the full problem, conical shapes are imposed as far-field boundary conditions and the domain is truncated at some large distance. A unique shape $H(\zeta)$, with two corresponding far-field cone slopes, was thus found from (4.8) (figure 12). We note briefly that solving equation (4.8) with a shooting method proved unsuccesful due to numerical sensitivity. This is exacerbated by the fact that the singular point $\zeta = 0$ of (4.8), a natural starting point for the evaluation

https://doi.org/10.1017/S0022112003006736 Published online by Cambridge University Press

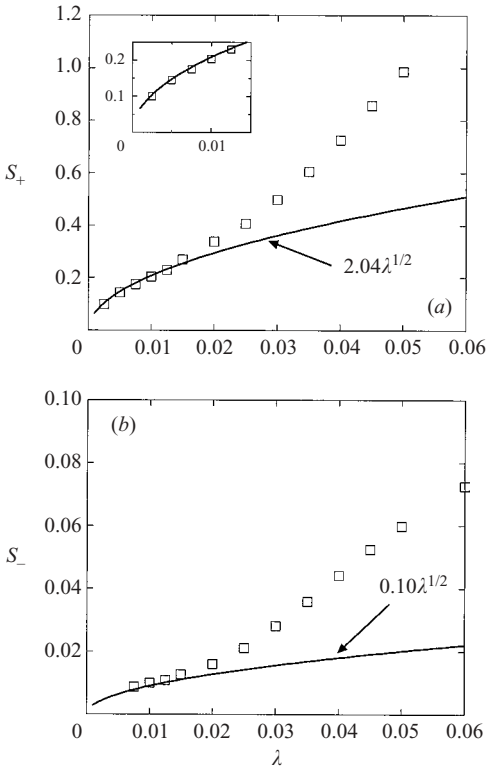


FIGURE 13. The slopes S_+ and S_- of the steep and shallow cones for $\lambda \ll 1$. The shallow cone slopes S_- were not fully resolved for $\lambda < 0.0075$ and are therefore not shown. The asymptotic scaling of $\lambda^{1/2}$ from the solution of (4.8) is also shown.

of forward and backward solutions (Brenner, Shi & Nigel 1994), lies away from the pinching neck $\zeta = 0.84$ and well into the region where the shape of the drop appears almost conical ($\zeta = 0$, $H = 0.508$, $H' = -0.719$, $H'' = -0.00092$).

By rescaling the axial coordinate of the full Stokes solution by $(8\lambda)^{-1/2}$ and using Galilean invariance, we obtain a λ-independent shape that can be directly compared with the asymptotic solution of equation (4.8). Figure 12 presents this asymptotic solution for $\tilde{C} = 1$, compared with the rescaled solution for the full problem and $\lambda = 0.015$; the agreement is indeed very good for this small value of λ. The asymptotic slopes for the far-field cones are calculated from (4.8) to be $2.04\lambda^{1/2}$ and $0.10\lambda^{1/2}$ for the steep and the shallow cone, respectively. These asymptotic results are plotted in figure 13 and compared with the numerically calculated slopes for values of λ less than 0.05. The agreement is good only for very small values of λ (notably for $\lambda < 0.02$); and although the $\lambda^{1/2}$ scaling is not obvious from the numerical results alone, since only a small number of data points is available for such small λ, the calculated values of both slopes are in very good quantitative agreement with those predicted from the one-dimensional model.

Note again that the asymptotic one-dimensional approximation is only expected to be accurate for flow in a thin thread, i.e. both cone angles should be sufficiently small. Although the slopes of the cones are predicted to decrease as $\lambda^{1/2}$, there is a marked asymmetry between the two sides: the steep cone is about 20 times larger than the shallow cone and thus, even for relatively small values of λ, the steep cone angle is

https://doi.org/10.1017/S0022112003006736 Published online by Cambridge University Press

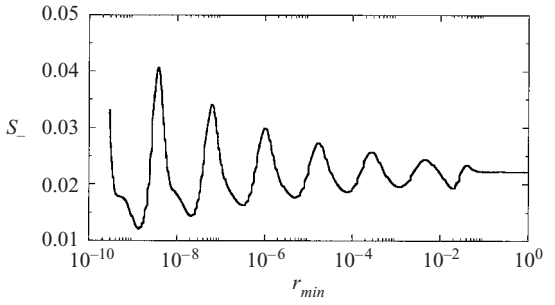


FIGURE 14. The slope of the shallow cone S_- plotted as a function of the minimum radius r_{min} for a time-dependent run and $\lambda = 34$. Small perturbations to the steady similarity solutions grow into nonlinear oscillations. The minimum radius is used as a convenient proxy for τ, the time to pinch-off (see Lister & Stone 1998).

still sizeable (according to the asymptotic scaling it only reaches 5° when λ is as small as 0.0018).

5. Stability

The direct calculation of the self-similar solution has allowed the expansion of previous time-dependent results to both smaller and larger values of the viscosity ratio λ. Zhang & Lister (1999) observed that for $\lambda > 16$ (e.g. $\lambda = 32$) the evolution of the thread became oscillatory and self-similar shapes could not be extracted from the time-dependent solution. In time-dependent simulations the origin of τ (the time to pinch-off) can only be estimated; it is thus more convenient to use the minimum radius of the pinching neck $r_{min}(\tau)$, which scales linearly in τ, as a measure of the time remaining to pinching and hence as a scaling for self-similar shapes (see also Lister & Stone 1998). The calculation of Zhang & Lister (1999) is repeated here for $\lambda = 34$ with an initial shape close to the similarity solution of § 3, and the slope of the shallow cone at $R = 1000$ is plotted as a function of r_{min} in figure 14. The values of the slope are obviously oscillating, with a well-defined period and increasing amplitude. Similar oscillatory behaviour, but with decreasing amplitude, is observed for smaller values of λ, such as $\lambda = 28$, where converged solutions can be obtained with the time-dependent formulation. The experimental results of Cohen *et al.* (1999) and Cohen & Nagel (2001) are possibly also in agreement with an onset of oscillations, since they report that they were unable to calculate the cone slopes accurately for $\lambda > 26$.

Although direct solution of the similarity equations by Newton's method finds solutions that are steady in similarity space, it can also be used to determine the onset of time-dependent instabilities and their quantitative description. Consider q-dependent solutions of the evolution equation (2.8) given by small perturbations of the steady self-similar shape of the form

$$\tilde{F}(\bar{r}, \bar{z}, q) = \bar{F}(\bar{r}, \bar{z}) + \hat{F}(\bar{r}, \bar{z})\mathrm{e}^{\sigma q}. \tag{5.1}$$

Substitution of (5.1) into (2.8) leads to a linearized eigenvalue problem

$$\sigma \hat{F} = J\hat{F}, \tag{5.2}$$

where J is the Jacobian $\partial K/\partial F$ or $\partial K/\partial n$ calculated in the Newton iteration scheme and the eigenvector $\hat{F}$ describes a self-similar eigenmode of the self-similar shape. The Jacobian is calculated numerically from small perturbation to the normal of

https://doi.org/10.1017/S0022112003006736 Published online by Cambridge University Press

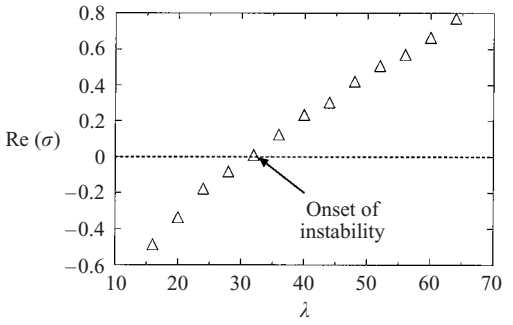


FIGURE 15. The real part of the least-stable eigenvalue σ of the self-similar Jacobian as a function of the viscosity ratio λ.

the interface. Note also that $e^{\sigma q} = \tau^{\sigma}$ so that the eigenvalues σ, as obtained from (5.2), correspond to exponents of an algebraic dependence on the time to pinch-off. The eigenvalues and associated eigenvectors were thus calculated for all values of λ where similarity solutions were available; for a given numerical discretization with N_p points, N_p eigenmodes were obtained. (We restrict our analysis to axisymmetric eigenmodes, since we would expect non-axisymmetric perturbations to decay under the stabilizing effects of the azimuthal curvature.)

Care is needed when interpreting the eigenvalue spectrum of the linear stability problem (Witelski & Bernoff 1999; Leppinen & Lister 2003). In addition to any physically unstable modes, there can also be positive eigenvalues associated with symmetry modes such as invariance under spatial and temporal translations. Although such modes have positive eigenvalues, they do not represent true instabilities, but simply the fact that solutions with different pinch-off positions or critical times appear to diverge exponentially in the similarity variable frame. For the case of viscous pinch-off (see Leppinen & Lister 2003 for the case of inviscid pinch-off) there are two such symmetry modes associated with a shift in the time origin and a shift in the axial location of pinch-off. Both have eigenvalues equal to 1 since $r \sim z \sim \tau$. For all values of λ these modes could easily be identified in the Jacobian and their eigenvalues verified. (Since the calculations actually use a timescale defined by C, shown in (2.7), the numerical Jacobian produces eigenvalues also multiplied by C.) It was further found that for $\lambda < 32$ all eigenvalues, with the exception of the symmetry modes referred to above, had negative real parts indicating that the steady solutions are stable. However, for $\lambda \approx 32$ a pair of eigenvalues with a positive real part is first calculated, which marks the onset of an oscillatory instability that persists for $\lambda > 32$, in agreement with the behaviour observed in the time-dependent simulations. Figure 15 presents the real part of the least stable eigenvalue σ as a function of λ; it is apparent that it becomes positive (unstable) near $\lambda = 32$. Owing to the small slope of this curve and the numerical errors associated with discretization, we estimate the critical value of λ as 32 ± 0.5.

In addition to the stability limit, the real and imaginary parts of the least stable eigenvalue give information relating to the rate of decay or increase of the oscillations and their periodicity. To demonstrate quantitative agreement between the stability analysis and the time-dependent behaviour the case $\lambda = 20$ is studied in more detail. This value of λ is sufficiently large that oscillatory behaviour is easily demonstrated and sufficiently small that the system remains stable and the time-dependent solution can be easily evaluated. Again following the time-dependent approach of Zhang

https://doi.org/10.1017/S0022112003006736 Published online by Cambridge University Press

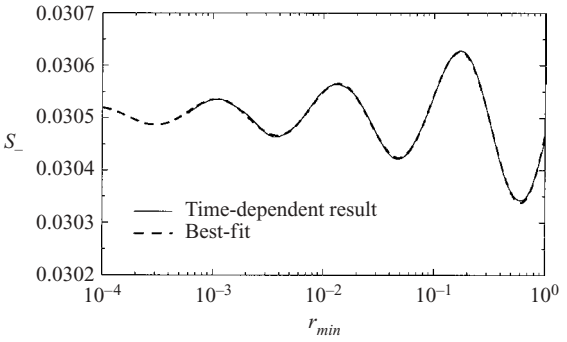


FIGURE 16. The slope of the shallow cone S_- is plotted as a function of the minimum radius r_{min} for a time-dependent run and $\lambda = 20$. A best-fit of the form $C_1 + C_2 \exp(C_3 \ln(r_{min}) \cos(C_4 \ln(r_{min}) + C_5)$ is also shown. The asymptotic shape C_1, decay rate C_3 and frequency C_4 agree with the similarity theory.

& Lister (1999) the shape of the interface was calculated as a function of the time to pinch-off (or equivalently, as a function of the minimum radius), and the resulting angle of the shallow far-field cone is plotted in figure 16. Damped oscillatory behaviour is evident which is described to great accuracy by a best-fit of the form $C_1 + C_2 \exp C_3 \ln(r_{min}) \cos(C_4 \ln(r_{min}) + C_5)$. The amplitude C_2 and phase C_5 depend on initial conditions. The fitted values $C_3 = 0.28$ and $C_4 = 2.48$, describing the rate of decay and period of the oscillations, correspond to the real and imaginary part of the least stable eigenmode of the system, and can thus also be calculated from the eigenvalues of the self-similar solution, giving values of $C_3 = 0.29$ and $C_4 = 2.46$ respectively. The two independently calculated sets of constants are thus in very good agreement, verifying the stability analysis and the connection between the self-similar and the time-dependent solutions. (The eventual steady far-field slope C_1 is also in excellent agreement between the two approaches.) Similar agreement is expected to hold close to the steady solution for all values of λ though exact quantitative comparisons are not always possible numerically: for small λ the fluctuations decay very rapidly and are hard to quantify, while for unstable λ the calculation of the time-dependent solution becomes computationally expensive and soon deviates into a nonlinear regime.

6. Conclusions

The effect of the viscosity ratio on the pinch-off of axisymmetric viscous drops has been studied in detail. Similarity variables were introduced and converged self-similar shapes were calculated directly, by combining a boundary-integral method with an iterative procedure. This approach allowed us to expand on previous time-dependent results (Zhang & Lister 1999) and study a wide range of viscosity ratios λ and, in particular, the previously unresolved limits of $\lambda \ll 1$ and $\lambda \gg 1$. The self-similar profiles are always asymmetric and are characterized by a double cone structure far away from the pinching neck, with both cone angles smaller than 90°.

For $\lambda \gg 1$ (corresponding to a very viscous fluid pinching in air) the self-similar shapes have a very steep cone on one side of the pinching neck and a very shallow one on the other. This trend contrasts with the symmetric predictions of the long-wavelength calculation for $\lambda = \infty$ of Papageorgiou (1995) and suggests that the presence of the external fluid remains asymptotically important even for $\lambda \gg 1$ owing

https://doi.org/10.1017/S0022112003006736 Published online by Cambridge University Press

to the non-commutation of the limits $\lambda \to \infty$ and $\tau \to 0$. The slopes of the steep and the shallow cone are determined as a function of λ and the existence of at least two distinct lengthscales in the solution is demonstrated. While no theoretical explanation is offered for the λ dependence of the steep cone, the shallow cone slope appears to follow the simple slender-body analysis of Lister & Stone (1998). A simplified model that accurately describes the pinching of a very viscous thread in the presence of a less viscous ambient fluid has yet to be developed; our data could, however, serve as a useful comparison for future studies.

For $\lambda \ll 1$ (corresponding to an elongated bubble pinching in a viscous fluid) the self-similar shape has a very shallow cone on either side of the pinching neck. A simple one-dimensional long-wavelength model is thus developed and a $\lambda^{1/2}$ scaling is found for the slopes of the two shallow cones. This simple model is in good quantitative agreement with the solution of the full problem; sufficiently small values of λ need to be sampled, however, for the asymptotic limit to be reached, since the slopes of the two cones remain very asymmetric for all λ.

Finally, the self-similar formulation has been used to study the stability of the time-dependent solution. The eigenvalues of the Jacobian of the iterative scheme were calculated and simply correlated with fluctuations in the time-dependent solution. The time-dependent solutions are found to be stable for all viscosity ratios, $0 < \lambda < 32$, while the onset of oscillatory instabilities is observed for $\lambda > 32$. It is not clear how pinch-off is attained for $\lambda > 32$; oscillatory instabilities would make an experimental investigation prohibitively difficult.

The slender neck and shallow cone of the self-similar shape are potentially subject to the mechanisms of secondary Rayleigh instability (cf. Brenner *et al.* 1994, 1996) and of necking instability, since the viscous interior is under tension. These mechanisms would normally lead to a direct instability (Tomotika 1936), whereas the fact that the instability is oscillatory suggests that at least one other effect plays a role. We note also the complications of long-range interactions in Stokes flow, and leave detailed investigation of pinch-off for $\lambda > 32$ for future work.

Financial support from the EPSRC and the Newton Trust is gratefully acknowledged.

Appendix

The calculation of separable solutions for Stokes flow in two infinite viscous cones (of viscosity $\lambda\mu$ and surface tension γ), submerged in a viscous fluid (of viscosity μ) is outlined here. Solutions correspond to an instantaneous Stokes flow (no time dependence) and the cone angles (θ_1, θ_2, where both angles in this Appendix are measured from $\theta = 0$) are assumed fixed. The axisymmetric Stokes stream function, $\Psi(R, \theta)$, satisfies the biharmonic equation

$$\nabla^4 \Psi = \left[\frac{\partial^2}{\partial R^2} + \frac{1-\xi^2}{R^2} \frac{\partial^2}{\partial \xi^2} \right]^2 \Psi = 0,$$

where (R, θ) are spherical polar coordinates, $\xi = \cos\theta$, and the velocity components are given by

$$u_R = -\frac{1}{R^2} \frac{\partial \Psi}{\partial \xi}, \qquad u_\theta = -\frac{1}{R(1-\xi^2)^{1/2}} \frac{\partial \Psi}{\partial R}.$$

https://doi.org/10.1017/S0022112003006736 Published online by Cambridge University Press

On the surface of both cones, the velocity components and the shear stress are continuous. Thus

$$[u_R]_S = 0, \qquad [u_\theta]_S = 0 \quad \text{at } \theta = \theta_{1,2}, \tag{A 1a, b}$$

$$\left[\frac{1}{R}\frac{\partial u_R}{\partial \theta} + \frac{\partial u_\theta}{\partial R} - \frac{u_\theta}{R}\right]_S = 0 \quad \text{at } \theta = \theta_{1,2}, \tag{A 2}$$

while the normal-stress jump balances the surface tension

$$\left[-p + 2\mu_{1,2}\left(\frac{u_R}{R} + \frac{1}{R}\frac{\partial u_\theta}{\partial \theta}\right)\right]_S = \gamma\frac{\cos\theta\sin\theta}{R} \quad \text{at } \theta = \theta_{1,2}, \tag{A 3}$$

where $[\,]_S$ denotes the interfacial jump, $\mu_{1,2}(=\lambda\mu$ or $\mu)$ refers to the viscosities of the two fluids, and the interfacial curvature is that of a perfect cone.

The motion of the two fluid cones is driven by surface tension, an $O(1/R)$ term, which corresponds to an $O(R^2)$ or $O(R^2\ln R)$ term for the stream function. A general separable expression for Ψ is thus (Happel & Brenner 1973)

$$\Psi = R^2\ln R f(\xi) + R^2 g(\xi),$$

where $f(\xi)$ and $g(\xi)$ are general solutions of the ordinary differential equations

$$(1-\xi^2)f'' + 2f = 0, \qquad [(1-\xi^2)g'' + 2g + 3f]'' = 0. \tag{A 4a, b}$$

The general solution of (A 4*a*) is

$$f(\xi) = A_1(1-\xi^2) + A_2\left(\frac{1}{2}(1-\xi^2)\ln\frac{1+\xi}{1-\xi} + \xi\right).$$

Continuity of the logarithmic term in the velocity implies that both A_1 and A_2 take the same values in the two cones and in the surrounding fluid. Exclusion of singularities at $\xi = \pm 1$ thus implies that $A_2 = 0$ in all three regions.

The solution of (A 4*b*) is then

$$g(\xi) = -A_1 - \frac{1}{2}A_1(1-\xi^2) + \frac{1}{2}A_1(1-\xi^2)\ln(1-\xi^2) + C_1\xi + C_1\frac{1}{2}(1-\xi^2)\ln\frac{1+\xi}{1-\xi} + C_2(1-\xi^2) + C_3\xi + C_4,$$

where the constant coefficients C_1, C_2, C_3 and C_4 are in general different in the two cones and the surrounding fluid; the superscripts r, l and c will be used hereafter to refer to coefficients corresponding to the 'right-hand' cone ($0 < \theta < \theta_1$), the 'left-hand' cone ($\theta_2 < \theta < \pi$) and the 'central' surrounding fluid ($\theta_1 < \theta < \theta_2$). In the right-hand cone, which includes $\theta = 0$ ($\xi = 1$), it is also required (to avoid singularities) that

$$C_1^r = A_1, \qquad C_4^r = -C_3^r,$$

while in the left-hand cone, which includes $\theta = \pi$ ($\xi = -1$),

$$C_1^l = -A_1, \qquad C_4^l = C_3^l.$$

This leaves nine unknowns (A_1, C_2^r, C_3^r, C_2^l, C_3^l, C_1^c, C_2^c, C_3^c, C_4^c) to be determined by the eight boundary conditions given by matching velocities and stresses on the fluid interfaces according to (A 1)–(A 3). These boundary conditions are sufficient to determine A_1, C_3^r, C_3^l, C_1^c, C_3^c, C_4^c, while C_2^r, C_2^l and C_2^c can be determined to within the same additive constant. Note that C_2 simply corresponds to axial translation and a constant translational velocity (in the absence of inertia) can always be included.

https://doi.org/10.1017/S0022112003006736 Published online by Cambridge University Press

The first coefficient is given by

$$A_1 = -\frac{1}{4}\frac{\xi_2\left(1-\xi_2^2\right)^{1/2}+\xi_1\left(1-\xi_1^2\right)^{1/2}}{2\lambda+(1-\lambda)\left(\xi_1^3-\xi_2^3\right)}, \tag{A 5}$$

where $\xi_1 = \cos\theta_1$ and $\xi_2 = \cos\theta_2$.

From the above solutions in spherical polar coordinates it is straightforward to calculate the radial and axial velocities on the surfaces of the two cones in cylindrical polar coordinates. These are

$$u_r = -\frac{(1-\xi^2)^{1/2}}{R^2}\frac{\partial\Psi}{\partial\xi} - \frac{\xi}{R(1-\xi^2)^{1/2}}\frac{\partial\Psi}{\partial R}, \tag{A 6a}$$

$$u_z = -\frac{\xi}{R^2}\frac{\partial\Psi}{\partial\xi} + \frac{1}{R}\frac{\partial\Psi}{\partial R}, \tag{A 6b}$$

where u_r, r refer to radial components in cylindrical polar coordinates and u_R, R refer to radial components in spherical polars. Using the solution for Ψ, (A 6) can be rewritten as

$$u_r = \begin{cases} -\dfrac{\left(1-\xi_1^2\right)^{1/2}}{1+\xi_1}\left(2A_1 + C_3^r(1-\xi_1)\right) & \text{for} \quad \xi = \xi_1 \\ -\dfrac{\left(1-\xi_2^2\right)^{1/2}}{1-\xi_2}\left(-2A_1 + C_3^l(1+\xi_2)\right) & \text{for} \quad \xi = \xi_2, \end{cases} \tag{A 7a}$$

$$u_z = \begin{cases} 2A_1\ln R + 2A_1\ln(1+\xi_1) + 2C_2^r + C_3^r(\xi_1-2) & \text{for} \quad \xi = \xi_1 \\ 2A_1\ln R + 2A_1\ln(1-\xi_2) + 2C_2^l + C_3^l(\xi_2+2) & \text{for} \quad \xi = \xi_2. \end{cases} \tag{A 7b}$$

The constant values of u_r on each cone, the coefficient of $\ln R$ in u_z and the difference in the constant terms in u_z are all in good quantitative agreement with the far-field velocities in the numerically determined similarity solutions for pinch-off.

REFERENCES

Brenner, M. P., Lister, J. R. & Stone, H. A. 1996 Pinching threads, singularities and the number 0.0304... *Phys. Fluids* **8**, 2827–2836.

Brenner, M. P., Shi, X. D. & Nigel, S. R. 1994 Iterated instabilities during droplet fission. *Phys. Rev. Lett.* **73**, 3391–3394.

Chen, M. P. & Steen, H. A. 1997 Dynamics of inviscid capillary breakup: Collapse and pinchoff of a film bridge. *J. Fluid Mech.* **341**, 245–267.

Cohen, I., Brenner, M. P., Eggers, J. & Nagel, S. R. 1999 Two fluid drop snap-off problem: Experiments and theory. *Phys. Rev. Lett.* **83**, 1147–1150.

Cohen, I. & Nagel, S. R. 2001 Testing for scaling behavior dependence on geometrical and fluid parameters in the two fluid drop snap-off problem. *Phys. Fluids* **13**, 3533–3541.

Day, R. F., Hinch, E. J. & Lister, J. R. 1998 Self-similar capillary pinchoff of an inviscid fluid. *Phys. Rev. Lett.* **80**, 704–707.

Eggers, J. 1993 Universal pinching of 3d axisymmetric free-surface flow. *Phys. Rev. Lett.* **71**, 3458–3460.

Happel, J. & Brenner, H. 1973 *Low Reynolds Number Hydrodynamics*, 2nd edn. Noordhoff International Publishing.

Leppinen, D. & Lister, J. R. 2003 Capillary pinch-off in inviscid fluids. *Phys. Fluids* **15**, 568–578.

Lister, J. R. & Stone, H. A. 1998 Capillary breakup of a viscous thread surrounded by another viscous fluid. *Phys. Fluids* **10**, 2758–2764.

Papageorgiou, D. T. 1995 On the breakup of viscous liquid threads. *Phys. Fluids* **7**, 1529–1544.

Pozrikidis, C. 1999 Capillary instability and breakup of a viscous thread. *J. Engng Maths* **36**, 255–275.

https://doi.org/10.1017/S0022112003006736 Published online by Cambridge University Press

Rallison, J. M. & Acrivos, A. 1978 A numerical study of the deformation and burst of a viscous drop in an extensional flow. *J. Fluid Mech.* **89**, 191–200.

Stone, H. A. & Leal, L. G. 1990 The effect of surfactants on drop deformation and breakup. *J. Fluid Mech.* **220**, 161–186.

Taylor, G. I. 1964 Conical free surfaces and fluid interfaces. In *Proc. 11th Intl Cong. Theor. App. Mech.*, pp. 790–796. Munich.

Tomotika, S. 1936 Breaking up of a drop of viscous liquid immersed in another viscous fluid which is extending at a uniform rate. *Proc. R. Soc. Lond.* A **153**, 302–318.

Witelski, T. P. & Bernoff, A. J. 1999 Stability of self-similar solutions for van der waals driven thin film rupture. *Phys. Fluids* **11**, 2443–2445.

Zhang, W. W. & Lister, J. R. 1999 Similarity solutions for capillary pinch-off in fluids of differing viscosity. *Phys. Rev. Lett.* **83**, 1151–1154.

https://doi.org/10.1017/S0022112003006736 Published online by Cambridge University Press